PAPER

Determination of Work Function for p- and n-Type 4H-SiC Single Crystals via Scanning Kelvin Probe Force Microscopy

Determination of Work Function for p- and n-Type 4H-SiC Single Crystals via Scanning Kelvin Probe Force Microscopy

Hui Li(李辉)[1,3*], Guobin Wang(王国宾)[1,2], Jingyu Yang(杨靖宇)[1,2], Zesheng Zhang(张泽盛)[1], Jun Deng(邓俊)[1], and Shixuan Du(杜世萱)[1,3]

[1]*Beijing National Laboratory for Condensed Matter Physics, and Institute of Physics, Chinese Academy of Sciences, Beijing 100190, China*
[2]*University of Chinese Academy of Sciences, Beijing 100049, China*
[3]*School of Physical Sciences, University of Chinese Academy of Sciences, Beijing 100049, China*

(Received 9 September 2023; accepted manuscript online 19 October 2023)

Silicon carbide (SiC) is a promising platform for fabricating high-voltage, high-frequency and high-temperature electronic devices such as metal oxide semiconductor field effect transistors in which many junctions or interfaces are involved. The work function (WF) plays an essential role in these devices. However, studies of the effect of conductive type and polar surfaces on the WF of SiC are limited. Here, we report the measurement of WFs of Si- and C-terminated polar surfaces for both p-type and n-type conductive 4H-SiC single crystals by scanning Kelvin probe microscopy (SKPFM). The results show that p-type SiC exhibits a higher WF than n-type SiC. The WF of a C-terminated polar surface is higher than that of a Si-terminated polar surface, which is further confirmed by first-principles calculations. By revealing this long-standing knowledge gap, our work facilitates the fabrication and development of SiC-based electronic devices, which have tremendous potential applications in electric vehicles, photovoltaics, and so on. This work also shows that SKPFM is a good method for identifying polar surfaces of SiC and other polar materials nondestructively, quickly and conveniently.

DOI: 10.1088/0256-307X/40/12/128101

The work function (WF; $\Phi = E_{\rm vac} - E_{\rm f}$) is an important physical parameter and represents the minimum energy required to remove an electron from a material to vacuum.[1] The WF plays an important role in the fabrication of devices in which many junctions or interfaces are involved.[1] Recently, silicon carbide (SiC) single crystals have attracted increasing attention, thanks to their superior properties for fabricating higher-power devices such as metal oxide semiconductor field effect transistors (MOSFETs), Schottky barrier diodes (SBDs), and insulated gate bipolar transistors (IGBTs), which have tremendous potential applications in electric vehicles, photovoltaics, and so on.[2,3] The WF of SiC plays a crucial role in performance of these devices for formation of good Ohmic contact, determination of barrier height, etc.[4]

Currently, n-type 4H-SiC single crystals are the dominant platforms for fabricating these devices because wafer-scale (4–6 in) n-type 4H-SiC single crystals can be mass-produced via the commercially available physical vapor deposition (PVT) technique.[5] High-quality p-type 4H-SiC substrates with a low resistivity of $< 0.2\,\Omega{\cdot}$cm are also required for IGBTs to achieve higher blocking voltages (> 10 kV). However, the growth of p-type 4H-SiC via PVT remains a challenge. Fortunately, a recent breakthrough in the high-temperature solution growth (HTSG) technique provides wafer-scale (4–6 in) p-SiC single crystals with high crystalline quality and uniform Al doping in both the axial and radial directions.[6,7] The availability p-SiC single crystals enables the possibility of studying the effect of conductive type on the WF of 4H-SiC. As reported in 6H-SiC,[8] the WFs for n- and p-type SiC are slightly different. The WFs are therefore expected to be different for p- and n-type 4H-SiC, and this needs further study.

Additionally, the polar surfaces also have a noticeable impact on the WF of a polar material because the WF is typically composed of electron chemical potential and the surface dipole, which is affected by many factors including crystallographic orientation.[9] Thus, apart from the conductive type, polar properties also influence the WF and the performance of fabricated devices.[1,10–14] In ZnO, this has been proved to be the case. The WFs of ZnO (0001) and $(000\bar{1})$ polar surfaces are 3.15 ± 0.15 and 4.85 ± 0.15 eV, respectively.[12] Notably, 4H-SiC with a hexagonal crystal structure is a typical polar semiconductor, having Si-terminated (0001) and C-terminated $(000\bar{1})$ polar surfaces.[15] A Si-terminated (0001) polar surface is usually applied to grow SiC epitaxially for the fabrication of MOSFETs or IGBTs.[16] In these devices, Si- and C-terminated polar surfaces form interfaces with gate oxide, gate metal, and Ohmic metal electrode, respectively.[17] Thereby, precise determination of the WFs of Si- and C-terminated polar surfaces is especially important for fabrication of SBDs, MOSFETs, and IGBTs.

The widely applied methods for measurement of the WF are x-ray photoelectron spectroscopy (XPS) and ultraviolet photoelectron spectroscopy,[18,19] which require an ultra-high vacuum and high standards for sample

*Corresponding author. Email: lihui2021@iphy.ac.cn

preparation.[18,19] Compared with these methods, scanning Kelvin probe force microscopy (SKPFM) is a useful method for accurately measuring the WF. SKPFM is a non-destructive and quick method for measuring the WF of a material and can be conducted in an atmospheric environment.[20–22] It is less affected by surface properties such as roughness and scratches.[22] As shown in Fig. S1 of the Supporting Information, the contact potential difference (CPD) between the measured sample and the conductive atomic force microscope (AFM) tip can be obtained according to the equation[10,23]

$$V_{\mathrm{CPD}} = V_{\mathrm{tip}} - V_{\mathrm{sample}} = \frac{\phi_{\mathrm{tip}} - \phi_{\mathrm{sample}}}{e}. \quad (1)$$

Here, the WF of commercial 6-in n-type and 4-in p-type 4H-SiC grown via HTSG is studied by SKPFM. Our results show that the WF of p-type 4H-SiC is higher than that of the n-type. The WF of a C-terminated polar surface is higher than that of a Si-terminated polar surface, which is further confirmed by first-principles calculations. By precisely determining the WF of Si-terminated (0001) and C-terminated ($000\bar{1}$) polar surfaces for both n- and p-type 4H-SiC, we enable more convenient fabrication of SiC-based devices. Our work also provides a new and facile method for distinguishing the polar surfaces of SiC, which is quite easy and convenient to extend to other polar materials.

Methods. Four-inch p-type 4H-SiC single crystals with a C-terminated polar surface as the growth front were grown via the top-seeded solution growth (TSSG) technique in a medium-frequency induction heating furnace (see our published paper[7]). For a Si-terminated polar surface, the as-grown 4H-SiC ingot was sliced by a multi-wire cutting machine. Afterwards, the Si- and C-terminated polar surfaces underwent grinding and polishing. The polished SiC wafers were cleaned using alcohol and deionized water. The washed wafers were dried by high-purity (99.999%) N_2 gas. Commercial 4H-SiC n-type wafers (6-in SiC, Beijing Tankblue) with a N-doping concentration of $\sim 5.0 \times 10^{18}\,\mathrm{cm}^{-3}$ were directly applied to conduct SKPFM measurements. Au thin films deposited via electron beam thermal evaporation were applied to conduct SKPFM measurements to determine the exact WF of the conductive AFM tip.

The p- and n-type 4H-SiC wafers were characterized by Raman spectra on a laser Raman spectrometer to determine their polytypes. XPS was conducted to confirm that the Al doping in p-type SiC and Hall effect measurements were conducted at room temperature to determine the carrier concentration. SKPFM characterizations were performed on an AFM using a conductive SCM-PIT tip. The SKPFM measurements were conducted in a two-step mode (Fig. S1). The morphology of the SiC was first measured in contact mode. Afterwards, the conducting tip was lifted from the SiC surface and held at a constant distance from the sample to conduct the potential measurement.

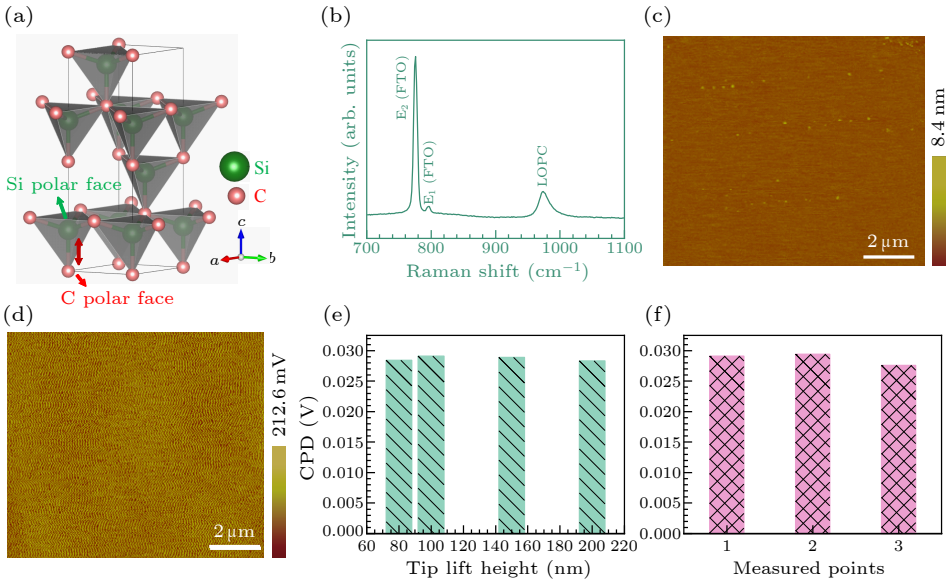

Fig. 1. Scanning Kelvin probe microscopy characterizations of the C-terminated polar surface of commercial 6-in n-type SiC grown by physical vapor deposition. (a) Schematic illustration of the crystal structure for 4H-SiC. The Si- and C-terminated polar surfaces are labeled. (b) Raman spectrum for n-SiC. (c) Atomic force microscope height image of the C-terminated polar surface. (d) Potential map of the C-terminated polar surface with a tip lift height of 100 nm. (e) Histogram of contact potential difference (CPD) with a tip lift height of 80, 100, 150, and 200 nm. (f) Histogram of CPD measured at different sample areas with a tip lift height of 100 nm.

The WF of Si- and C-terminated polar faces, energy bandgaps and projected density of states (PDOS) were calculated using density functional theory within projector-augmented wave potentials and the Perdew–Burke–Ernzerhof exchange-correlation functional[24] as implemented in the Vienna *ab initio* simulation package (VASP).[25,26] A plane-wave basis set with an energy cutoff of 550 eV was used. A Monkhorst–Pack[27] Brillouin zone sampling grid with a resolution of $0.02 \times 2\pi\,\text{Å}^{-1}$ was applied. In WF calculations of Si- and C-terminated polar

faces, the electric field in the vacuum was eliminated by back-to-back (b2b) methods.[28] For a slab, the top three layers of atoms closed to surface were optimized to match the surface characteristics. All the structures studied here were fully relaxed until forces converged to 0.01 eV/Å.

Results and Discussion. As is known, 4H-SiC is a non-centrosymmetric crystal with a space group of $P6_3mc$ and a point group of $6mm$,[29] indicating that it is a representative polar semiconductor. As shown in Fig. 1(a), 4H-SiC has C-terminated $(000\bar{1})$ and Si-terminated (0001) polar surfaces. The chemical bond orientation of the Si atom in the Si tetrahedron $\langle 0001 \rangle$ corresponds to the (0001) Si-terminated polar surface. The chemical bond orientation of the C atom in the carbon tetrahedron $\langle 000\bar{1} \rangle$ corresponds to the $(000\bar{1})$ C-terminated polar surface.

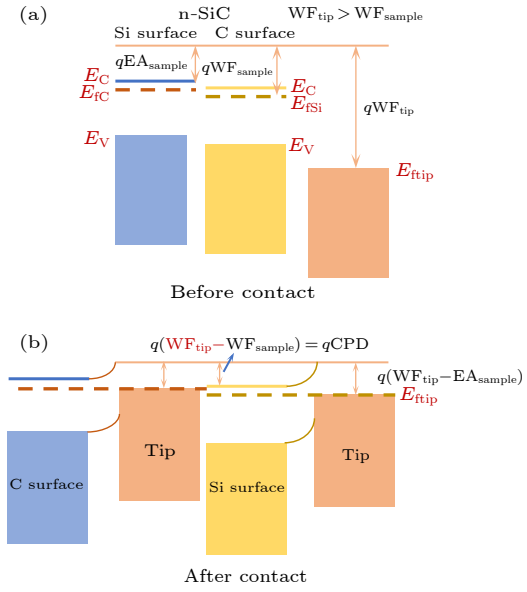

Fig. 2. Energy level alignment for n-SiC and a conductive tip: (a) before contact and (b) after contact.

The Raman spectrum, the fingerprint spectrum, is used to confirm the polytype of n-type SiC wafers. As shown in Fig. 1(b), all Raman peaks are in good agreement with 4H-SiC ones, indicating the 4H polytype.[30] The roughness of the C-terminated polar surface is 0.16 nm, determined from the height of the AFM image [Fig. 1(c)]. Seen from the AFM potential image [Fig. 1(d)], the CPD for the C-terminated polar surface is quite uniform. The measured CPD value between the conductive tip and C-terminated polar surface of n-SiC is 0.0284, 0.0291, 0.0289, and 0.0283 V when the tip lift height is 80, 100, 150, and 200 nm [Fig. 1(e)], respectively. We conducted SKPFM measurements on different areas (Fig. S2). The CPD between the conductive tip and C-terminated polar surface of n-SiC is 0.0291, 0.0294, and 0.0276 V with a tip lift height of 100 nm [Fig. 1(f)]. Therefore, it is seen that the CPD values are less dependent on the tip lift height and measured sample regions, showing the high reliability and high stability of SKPFM. CPD has a close relationship to the WF of the sample and AFM tip. The Au thin film with an assumed WF of 5.1 eV was measured via SKPFM to determine the WF of the conductive tip.[31] Figure S3 of the Supporting Information shows the measured results for Au film. Grain boundaries are clearly seen in the AFM height and amplitude error images [Figs. S3(a) and S3(b)]. However, the sample has nearly the same CPD in the grain interiors and grain boundaries [Fig. S3(c)]. Some scratches are also seen, which have little influence on the CPD values [Fig. S3(c)]. These results further illustrate the high reliability of SKPFM. The CPD values are 0.0266 V and 0.0243 V when the tip lift heights are 150 and 100 nm [Fig. S3(d)]. The WF for the conductive tip is calculated to be 5.1254 eV according to Eq. (1). For n-SiC and a conductive tip, the Fermi energy aligns to the same energy level after contact by electrons flowing from the n-SiC to the conductive tip (see Fig. 2). Thereby, the WF of a C-terminated polar surface is 5.0968 eV, calculated based on Eq. (1).

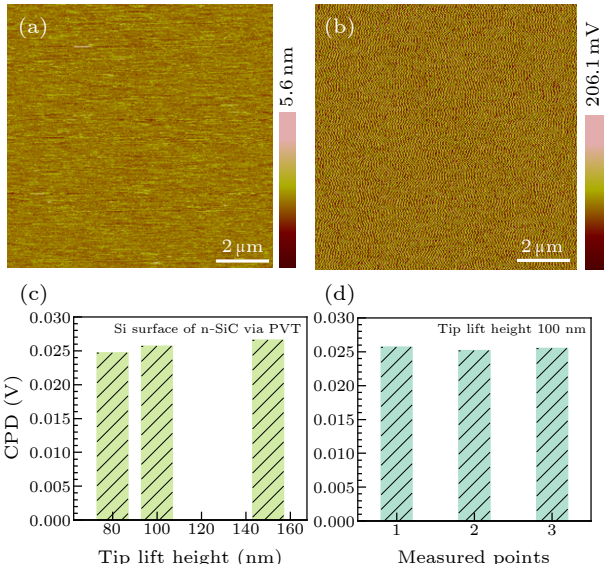

Fig. 3. Scanning Kelvin probe microscopy characterizations of the Si-terminated polar surface of commercial 6-in n-type SiC grown by physical vapor deposition. (a) Atomic force microscope height image of the Si-terminated polar surface. (b) Potential image of the Si-terminated polar surface with a tip lift height of 100 nm. (c) Histograms of CPD with tip lift heights of 80, 100, and 150 nm. (d) Histograms of CPD value measured at different sample areas with a tip lift height of 100 nm.

For the Si-terminated polar surface of n-type 4H-SiC, the surface roughness is 0.17 nm as characterized by the AFM [Fig. 3(a)]. Similarly, the CPD values for the Si-terminated polar surface are quite uniform [Fig. 3(b)]. The CPD is 0.0247, 0.0257, and 0.0266 V when the conductive tip lift height is 80, 100, and 150 nm [Fig. 3(c)]. The CPDs measured in three different regions (Fig. S4) are 0.0252, 0.0257, and 0.0255 V with a constant tip lift height of 100 nm [Fig. 3(d)]. The WF for the Si-terminated polar surface is calculated to be 5.0660 eV. Thus, the WFs for C- and Si-terminated polar surfaces of n-type 4H-SiC are 5.0968 and 5.0660 eV, respectively, indicating that the WF of the C-terminated polar surface is slightly higher than that of the Si-terminated polar surface.

As already mentioned, p-type SiC single crystal substrates are highly desired for the fabrication of IGBTs. Nevertheless, the growth of p-type SiC single crystals via PVT remains a big challenge because of the difference in vapor pressure of Al, Si, SiC_2, and Si_2C.[32] Compared with PVT, it is realized that HTSG, especially TSSG, can produce p-type SiC with uniform doping in both the radial and axial directions by the exploitation of Al-containing Si-based melts.[7] As a matter of fact, we have successfully grown 4-in p-type SiC single crystals via TSSG.[7] The results of Hall effect measurements (Fig. S5) show that the grown SiC is a p-type semiconductor with a carrier concentration of $2.2\times10^{20}\,\mathrm{cm}^{-3}$ and a resistivity of $0.12\,\Omega\cdot$cm. The resistivity is satisfactory for the requirements of practical applications ($<0.2\,\Omega\cdot$cm). XPS results (Fig. S6) confirm that the p-SiC is due to Al doping.[7,33] The full width at half maximum (FWHM) of the x-ray rocking curve for the as-grown surface is in the range of 32–43 arcsec,[7,33] indicating high crystalline quality of p-SiC. To the best of our knowledge, the resistivity of $0.12\,\Omega\cdot$cm and FWHM of 32–43 arcsec reported here are the best results for p-SiC single crystals.[34–36] To determine the polytype of SiC, Raman spectra were collected at seven random points from the as-grown surface of the SiC ingot [Fig. 4(a)]. Raman peaks located at 192.8, 203.6, 608.7, 776.0, 795.8, 831.2, and $960.2\,\mathrm{cm}^{-1}$ [Figs. 4(b) and 4(c)] are observed in the Raman spectra, which correspond to transverse acoustic (TA), longitudinal acoustic (LA), transverse optical (TO), and folded-longitudinal-optical (FLO) phonons and longitudinal-optical (LO) phonons, respectively, of 4H-SiC.[30] Thereby, the Raman spectra verify the 4H polytype of SiC. Step flows with a step height of 17–32 nm [Fig. 4(d), Fig. S7(a)] are obviously seen in the as-grown C-terminated polar surface, which is much smaller than 120 nm reported before, thanks to the optimization of growth parameters.[7] The surface steps have been reported to induce artefacts on the potential results.[37] To elucidate this, we performed SKPFM measurements directly on the as-grown surface of the SiC ingot [Fig. S7(a)]. As determined from the height and corresponding potential profiles [Figs. 4(d) and 4(e), Figs. S8 and S9], the surface steps have almost no impact on the SKPFM results. Since the tip lift height has little effect on the measured CPD, we lifted the tip 100 nm from the measured sample surface to keep the tip as close as the SiC surface as possible. Figure 4(f) displays a histogram of CPD measured at different regions of the sample (Fig. S10). The measured CPDs are 0.0190, 0.0185, 0.0186, and 0.0190 V, with an average value of 0.0188 V. Obviously, the CPD values are nearly the same, illustrating high accuracy and high stability of SKPFM.

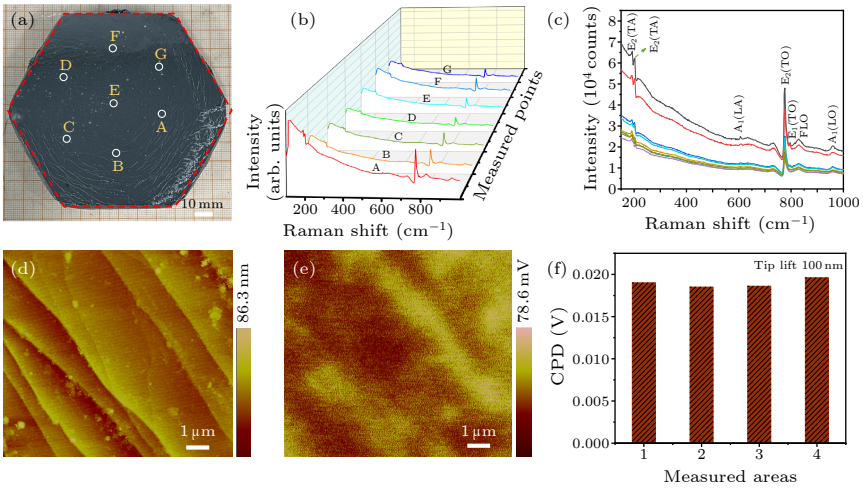

Fig. 4. Characterizations of the C-terminated polar surface of 4-inch p-type conductive SiC single crystals grown via top-seeded solution growth. (a) Photo of 4-in p-type conductive SiC single crystals and schematic illustration of the points for Raman measurement. [(b), (c)] Raman spectra of an as-grown 4-in p-SiC ingot. (d) Atomic force microscope height image and (e) potential image of an as-grown p-SiC ingot. (f) Histograms of contact potential difference measured with a tip lift height of 100 nm.

To exclude the effect of the tip on the measured WF of SiC, the Au thin film was further measured via SKPFM (see Fig. S11). The CPD is 0.0167 V when the tip lift height is 100 nm. Based on Eq. (1), the WF for the conductive tip is changed to 5.1167 eV. The WF for the C-terminated polar surface of p-type SiC is calculated to be 5.1334 eV, larger than that for n-SiC (5.0968 eV), showing similar results to other polar materials.[8] Apart from the step [Figs. 5(a) and 5(c)], a small trench marked by the arrow in Fig. 5(a) is also seen in the as-grown C-terminated polar surface. Interestingly, the CPD is nearly the same around the step and the trench [see Fig. 5(b)]. The as-grown C-surface was polished and measured via SKPFM. Figures 5(d) and 5(f) show the AFM height image and CPD image, respectively. The roughness of the polished surface is 0.5 nm. Some scratches are still seen. Similarly, the scratches have nearly no effect on the potential results [see Figs. 5(d)–5(g)]. The measured CPD values are 0.0221, 0.0222, and 0.0219 V when the tip lift heights are 80, 100, and 150 nm [Fig. 5(h)] and the mea-

sured CPD values are 0.0221, 0.0222, and 0.0211 V when the tip lift height is 100 nm [Fig. 5(i)] with an average value of 0.0219 V. To exclude the tip effect on the measured WF of SiC, the Au film was further measured via SKPFM. As shown in Fig. S12, the CPD is 0.0243 V when the tip lift height is 100 nm. The WF for the conductive tip is then calculated to be 5.1243 eV. Thus, the calculated WF for a polished C-terminated polar surface is 5.1462 eV, which is consistent with that of 5.1334 eV for an as-grown surface.

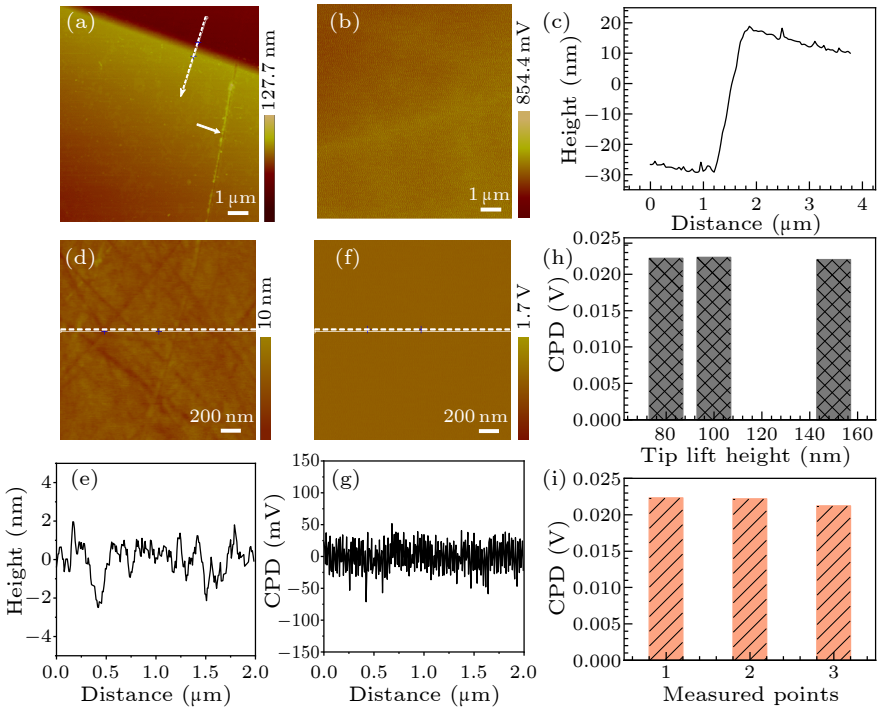

Fig. 5. Scanning Kelvin probe microscopy results for an as-grown and polished C-terminated polar surface for 4-in p-SiC grown via top-seeded solution growth. (a) AFM height map of the as-grown C-terminated surface. (b) Potential map of the as-grown C-terminated surface. (c) Height profile along the white line in panel (a). (d) AFM height image of a polished C-terminated polar surface. (e) Height profile along the white line in panel (d). (f) Potential map of a polished C-terminated polar surface. (g) Potential profile along the white line in panel (f). (h) Histogram of CPD measured with a tip lift height of 80, 100, and 150 nm for a polished C-terminated surface. (i) Histogram of CPD measured at different areas on the polished C-terminated polar surface with a tip lift height of 100 nm.

The polished Si-terminated polar surface with a surface roughness of 0.5 nm [Fig. 6(a)] was used to carry out SKPFM measurements. Some particles, indicated by the white arrow in Fig. 6(a), are seen in the polished surface. Determined from the corresponding CPD map [Fig. 6(b)], the particles have almost no impact on the measured CPD values. The measured CPD values are 0.0186, 0.0185, and 0.0183 V when the tip lift height is 80, 100, and 150 nm [Fig. 6(c)]. The CPD values measured at different regions are 0.0182, 0.0186, 0.0190, 0.0180, 0.0193, 0.0192, 0.0193, and 0.0186 V with an average value of 0.0187 V when the tip lift height is 100 nm [see Fig. 6(d)]. To verify that the wafering process does not affect the CPD of the Si face, we directly conducted SKPFM measurements on the unpolished Si-terminated polar surface. As shown in Fig. S13, the CPD is 0.0180 V, confirming that the wafering process has almost no influence on the CPD of the Si face. The WF of the tip will change due to wear after measuring for a long time. To exclude the effect of the tip on the measured CPD results, and thus the WF, the Au thin film was further measured via SKPFM. The measured CPD between the tip and the Au film is 0.0243 V with a tip lift height of 100 nm (Fig. S12). The WF for the conductive tip is then calculated to be 5.1243 eV based on Eq. (1). The WF for the Si-terminated polar surface of p-SiC is calculated to be $5.1243 + 0.0187 = 5.1430$ eV according to $(\mathrm{WF_{tip}} + \mathrm{CPD})/e$. Thus, it is seen that the WF of the Si polar surface is smaller than that of the C polar surface (5.1462 eV). The smaller WF for a Si-terminated polar surface is the case for both n- and p-type SiC. Similarly, the WF of the Ga polar surface is smaller than that of the N polar surface in GaN.[38] The negatively charged C causes a negative dipole (pointing inward) and a larger WF for the C-terminated polar surface, while the positively charged Si leads to a smaller WF.[39] In addition, our results show that the WF of p-type SiC is higher than that of n-type SiC. The increase in WF of SiC by p-type doping is in good agreement with the reported calculated results.[40] It is also well known that the WF for p-type doping is larger than that of n-type doping for the same semiconductor.[41,42] The Fermi level is lifted to be nearer to the vacuum energy for an n-type semiconductor while the Fermi level is lower for a p-type semiconductor based on classical band theory.[41,42] Thus, for the same semi-

conductor, the WF for the p-type is higher than that for the n-type. Thus, for fabricating devices on p-type SiC substrates, metals with much larger WF are necessary to form a good Ohmic contact.

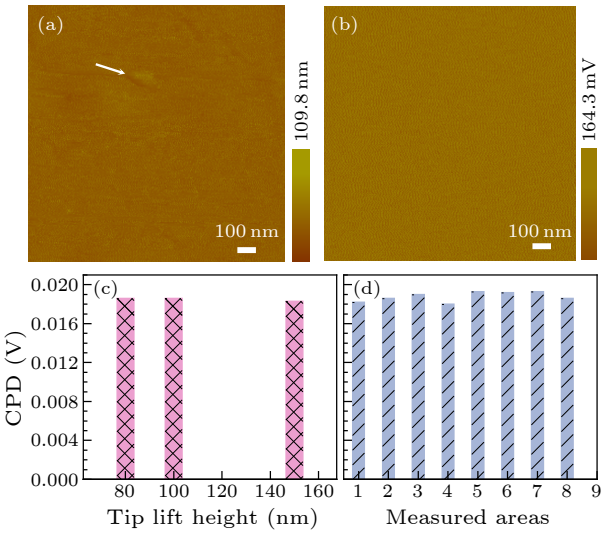

Fig. 6. Characterizations of a polished Si-terminated polar surface for 4-in conductive p-SiC grown via top-seeded solution growth. (a) Atomic force microscope height map of the polished Si-terminated polar surface. (b) Potential map of the polished Si-terminated polar surface. (c) Histogram of CPD measured with a tip lift height of 80, 100, and 150 nm. (d) Histogram of CPD measured eight times with a tip lift height of 100 nm.

Figure S14 shows the PDOS of Si- and C-terminated polar surfaces for 4H-SiC based on first-principles calculations. For both Si- and C-terminated polar surfaces, the thicknesses of the 4H-SiC layer and the vacuum layer are set to be 20 Å. The calculated band gap is 2.3 eV. At the center of the slab, the surface state fully decays and the band gap (from the PDOS) is the same as that of the bulk state, indicating sufficient thickness of the slab for the C- and Si-terminated polar surface calculations. Then, the position of the conduction band minimum (CBM) and valence band maximum (VBM) are calibrated through the PDOS in the central region (Fig. S14).

In order to theoretically obtain the WF of different surface terminations of 4H-SiC we establish two models, as shown in Fig. S14. Both Si- and C-terminated surface SiC models contain 16 layers of atoms. By optimizing the top three layers of atoms on the surface, stable configurations are obtained. The PDOSs were then calculated to verify that the models are large enough to simulate the crystal surfaces. The electrostatic potential based on these models is calculated to obtain the WFs. Due to the periodicity of VASP, two polar surfaces with different polarities will generate electrostatic fields in the vacuum, which is not conducive to calculation of the WF. Therefore, the b2b method[28] is used to eliminate the electric field in the vacuum. As shown in Fig. 7, the b2b method places surfaces with the same polarity facing each other. Then, the WF, ionization energy (IE) and electron affinity (EA) are obtained based on the energy differences between the electrostatic potential of the vacuum level and the Fermi level, VBM and CBM, respectively. The calculated WFs, IEs, and EAs of Si- and C-terminated polar surfaces are also shown in Fig. 7. The calculated WF, EA, and IE for the Si-terminated polar surface are 3.8, 2.9, and 5.2 eV, respectively [Fig. 7(a)]. The calculated WF, EA, and IE for the C-terminated polar surface are 5.6, 4.7, and 7.0 eV, respectively [Fig. 7(b)]. Therefore, the WF of the Si-terminated polar surface is smaller than that of the C-terminated polar surface, which qualitatively agrees with the experimental results. The large difference between the Si-terminated polar surface in experiment and calculation may be due to the differences in practical surfaces and the ideal surface built for the calculation.[43] Therefore, the WF obtained from SKPFM is a sensitive physical quantity for (0001)-orientated SiC (both n-type and p-type), which is insensitive to the surface roughness, impurity particles and scratches. This is always the case for SiC wafers grown via PVT and TSSG.

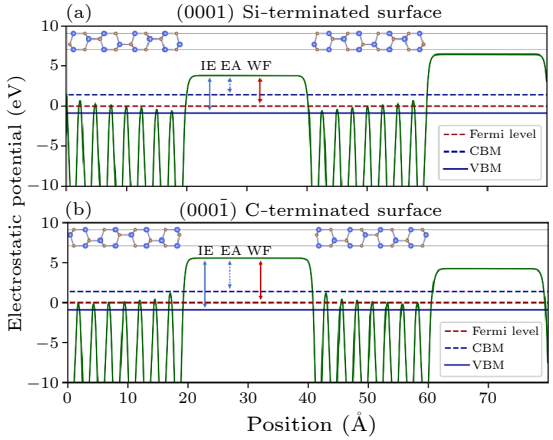

Fig. 7. Calculated electrostatic potential for Si- and C-terminated polar surfaces of 4H-SiC. (a) The calculated electrostatic potential for the Si-terminated polar surface of conductive 4H-SiC [work function (WF) 3.8 eV, electron affinity (EA) 2.9 eV, ionization energy (IE) 5.2 eV]. (b) The calculated electrostatic potential for the C-terminated polar surface of conductive 4H-SiC (WF 5.6 eV, EA 4.7 eV, IE 7 eV). The solid green line indicates electrostatic potential. The red dotted lines, the solid blue line and the blue dotted line represent the Fermi level, valence band minimum (VBM) and conduction band minimum (CBM), respectively.

In conclusion, we report an effective method for identification of the WF by SKPFM. The WF of p-type SiC is found to be larger than that of n-type SiC. The WF of a C-terminated polar surface is larger than that of a Si-terminated polar surface, which is confirmed by both the theoretical calculations and experimental results. Our work clarifies the influence of a polar surface and the conductive type on the WF of SiC, which is especially important for its application in devices. This method also works for other polar materials such as ZnO and GaN, because the WFs of the polar faces are always different. SKPFM is also a feasible method for determining polar surfaces of SiC and other polar semiconductors precisely, nondestructively, easily and simply.

Acknowledgments. This work was financially supported by the Beijing Municipal Science and Technology Project (Grant No. Z231100006023015), the Major Scientific and Technological Research and Development of Shunyi District of Beijing, and the Chinese Academy of Sciences.

References

[1] Shao G S 2021 *Energy Environ. Mater.* **4** 273
[2] Eddy C R and Gaskill D K 2009 *Science* **324** 1398
[3] La Via F, Alquier D, Giannazzo F, Kimoto T, Neudeck P, Ou H, Roncaglia A, Saddow S E E, and Tudisco S 2023 *Micromachines* **14** 1200
[4] Kimoto T and Cooper J A 2014 *Fundamentals of Silicon Carbide Technology: Growth, Characterization, Devices, and Applications* (New York: Wiley) p 189
[5] Wang G, Wang W J, Peng T H, Guo L W, and Chen X L 2018 *Science: HUMBLE BEGINNINGS, BRIGHT FUTURE Institute of Physics (CAS) at 90* p 51
[6] Wang G, Sheng D, Yang Y, Li H, Chai C, Xie Z, Wang W, Guo J, and Chen X 2023 *Energy Environ. Mater.* **0** e12678
[7] Wang G B, Sheng D, Li H, Zhang Z S, Guo L L, Guo Z G, Yuan W X, Wang W X, and Chen X L 2023 *CrystEngComm* **25** 560
[8] Pelletier J, Gervais D, and Pomot C 1984 *J. Appl. Phys.* **55** 994
[9] Greiner M T, Chai L, Helander M G, Tang W M, and Lu Z H 2012 *Adv. Funct. Mater.* **22** 4557
[10] Hutchison J A, Liscio A, Schwartz T, Canaguier-Durand A, Genet C, Palermo V, Samori P, and Ebbesen T W 2013 *Adv. Mater.* **25** 2481
[11] Li L K, Jurkovic M J, Wang W I, Van Hove J M, and Chow P P 2000 *Appl. Phys. Lett.* **76** 1740
[12] Marien J 1976 *Phys. Status. Solidi A* **38** 513
[13] Sumiya M, Yoshimura K, Ito T, Ohtsuka K, Fuke S, Mizuno K, Yoshimoto M, Koinuma H, Ohtomo A, and Kawasaki M 2000 *J. Appl. Phys.* **88** 1158
[14] Tang C G, Ang M C Y, Choo K K, Keerthi V, Tan J K, Syafiqah M N, Kugler T, Burroughes J H, Png R Q, Chua L L, and Ho P K H 2016 *Nature* **539** 536
[15] Zhong W W, Huang Y F, Gan D, Xu J Y, Li H, Wang G, Meng S, and Chen X L 2016 *Phys. Chem. Chem. Phys.* **18** 28033
[16] Musolino M, Carria E, Crippa D, Preti S, Azadmand M, Mauceri M, Isacson M, Calabretta M, and Messina A 2023 *Microelectron. Eng.* **274** 111976
[17] Kimoto T 2015 *Jpn. J. Appl. Phys.* **54** 040103
[18] Chen Y, Gong L, Du X, Chen S, Xie W, Zhang W, Chen J, and Xie F 2018 *J. Instrum. Anal.* **37** 796 (in Chinese)
[19] Kennou S 1995 *J. Appl. Phys.* **78** 587
[20] de Wit J H W 2004 *Electrochim. Acta* **49** 2841
[21] Koley G and Spencer M G 2001 *J. Appl. Phys.* **90** 337
[22] Li H, Liu X X, Lin Y S, Yang B, and Du Z M 2015 *Phys. Chem. Chem. Phys.* **17** 11150
[23] Jaramillo R and Ramanathan S 2011 *Adv. Funct. Mater.* **21** 4068
[24] Paier J, Hirschl R, Marsman M, and Kresse G 2005 *J. Chem. Phys.* **122** 234102
[25] Kresse G and Furthmuller J 1996 *Comput. Mater. Sci.* **6** 15
[26] Kresse G and Furthmuller J 1996 *Phys. Rev. B* **54** 11169
[27] Monkhorst H J and Pack J D 1976 *Phys. Rev. B* **13** 5188
[28] Beattie J M A, Goss J P, Rayson M J, and Briddon P R 2021 *J. Phys. Condens. Matter.* **33** 165003
[29] Wang S C, Zhan M J, Wang G, Xuan H W, Zhang W, Liu C J, Xu C H, Liu Y, Wei Z Y, and Chen X L 2013 *Laser Photonics Rev.* **7** 831
[30] Nakashima S, Harima H, and Solidi P S 1997 *Phys. Status Solidi A* **162** 39
[31] Luo M, Wu F, Long M, and Chen X 2018 *Nanotechnology* **29** 444001
[32] Müller R, Künecke U, Weingärtner R, Schmitt H, Desperrier P, and Wellmann P J 2004 *Mater. Sci. Forum* **483** 31
[33] Wang G, Li H, Sheng D, Wang W, and Chen X 2022 *J. Synth. Cryst.* **51** 3 (in Chinese)
[34] Eto K, Suo H, Kato T, and Okumura H 2017 *J. Cryst. Growth* **470** 154
[35] Xie X J, Sun L, Chen X F, Yang X L, Hu X B, and Xu X G 2019 *Scr. Mater.* **167** 76
[36] Zhong G L, Xie X J, Wang D S, Wang X L, Sun L, Yang X L, Peng Y, Chen X F, Hu X B, and Xu X G 2022 *CrystEngComm* **24** 7861
[37] Rohwerder M and Turcu F 2007 *Electrochim. Acta* **53** 290
[38] Lorenz P, Haensel T, Gutt R, Koch R J, Schaefer J A, and Krischok S 2010 *Phys. Status Solidi B* **247** 1658
[39] Hu G, Fung V, Huang J, and Ganesh P 2021 *J. Phys. Chem. Lett.* **12** 2320
[40] Zhang L and Cui Z 2022 *Front. Mater.* **9** 956675
[41] Monfort O and Plesch G 2018 *Environ. Sci. Pollut. R.* **25** 19362
[42] Yang X, Gan H, Tian Y, Peng L, Xu N, Chen J, Chen H, Deng S, Liang S D, and Liu F 2017 *Sci. Rep.* **7** 13057
[43] Lin L, Jacobs R, Chen D, Vlahos V, Lu-Steffes O, Alonso J A, Morgan D, and Booske J 2022 *Adv. Funct. Mater.* **32** 2203703